Bragg-like interference in one-dimensional double-period quasicrystals

Y. H. Cheng, C. H. Chang, C. H. Chen, and W. J. Hsueh*

Photonics Group, Department of Engineering Science and Ocean Engineering, National Taiwan University, 1, Sec. 4, Roosevelt Road, Taipei, 10660, Taiwan

(Received 10 April 2014; published 18 August 2014)

Three quasi-Bragg conditions (QBCs) in one-dimensional double-period quasicrystals based on high reflectance from interference are proposed. Analytical formulas for these QBCs are derived using band-edge equations. All of these QBCs have conditions that are different from that of the traditional Bragg condition. The QBC at quarter-wave thickness in double-period quasicrystals is also discontinuous in different regions of the gap map. In contrast, the traditional Bragg condition for periodic cases, which lies at quarter-wave thickness, is continuous in different regions of the gap map. It is found that there are three thickness conditions with the maximum reflectance occurring in the midpoints of the QBCs in double-periodic quasicrystals, which is analogous to the quarter-wave thickness in traditional periodic crystals. These QBCs in double-period cases are different not only from the traditional Bragg condition in periodic cases, but also from those in Fibonacci and Thue-Morse quasicrystals.

DOI: 10.1103/PhysRevA.90.023830 PACS number(s): 42.79.Fm, 61.44.Br, 78.67.Pt

I. INTRODUCTION

Bragg interference is one of the most important characteristics in traditional periodic structures [1,2]. This condition plays a key role in many important optical devices, such as resonators, lasers, filters, reflectors, and fiber Bragg gratings [3–5]. The recent discovery of quasicrystals has led to an increasing interest in their optical and electronic properties [6–10]. The transmission properties of electromagnetic waves in quasicrystals, such as their cycling and self-similar transmission spectra and their branching band structures, which are different from the periodic or aperiodic cases [11–15], are suited to optical devices that use advanced materials. Applications of traditional photonic crystals, such as laser action and Anderson localization of light can also be expected in quasicrystals with similar functionalities but significant flexibility [16]. Research has shown that a Bragg condition exists in a traditional periodic system, but it is absent in a disordered system. In contrast, field localization and delocalization occur in a disordered system and quasicrystals [17]. Whether Bragg conditions exist in quasicrystals is an interesting topic.

Since one-dimensional structures have attracted special attention because of their fundamental physics and their ease of fabrication for any wavelength scale, studies of one-dimensional traditional photonic crystals, disordered structures, and quasicrystals, such as Fibonacci, double-period, and Thue-Morse superlattices, have been undertaken [18–22]. Recently, two quasi-Bragg conditions (QBCs) with significant reflectances due to interference, which are analogous to one traditional Bragg condition for periodic cases [23,24], that occur in a Fibonacci superlattice have been proposed [19]. More recently, researchers have shown that there are three QBCs in Thue-Morse quasicrystals [25]. The Thue-Morse superlattice has a complete transmittance at its QBC for quarter-wave thickness. This is different from the QBCs in a Fibonacci superlattice and the traditional Bragg condition for periodic cases. Moreover, both the number and the conditions for QBCs in Fibonacci and Thue-Morse superlattices are different.

A double-period superlattice (DPSL) is a typical quasicrystal, alongside Fibonacci and Thue-Morse superlattices, and is of great importance [26,27]. Studies about the scaling property, self-similarity, localized states, and oblique incidence for a double-period superlattice have been conducted [26,28]. Moreover, the properties of this superlattice with one of the media being a negative refractive index also have been investigated [27,29]. However, most of the studies only concentrate on the quarter-wave condition. To the authors' best knowledge, there have been few studies concerning the existence of QBCs in DPSLs with different thickness filling factors. It remains unclear whether QBCs exist in a double-period superlattice. Since the interference not only depends on an iteration rule, but also on the thickness and frequency, it cannot be simply derived from an iteration rule. If QBCs exist in a double-period superlattice, are they similar to Thue-Morse or Fibonacci superlattices or even to traditional bilayer periodical superlattices (BPSLs)? If the QBC exists, can these conditions be expressed as simple analytical forms? These questions are important not only to the basic optical physics in a DPSL, but also for the potential applications, such as multichannel filters, division multiplexing systems, photonic integrated circuits, and random lasers of the different types of quasicrystals [30,31].

In this study, a one-dimensional double-period dielectric superlattice is studied using the transmission spectra and a gap map method. The band-edge equation is used to determine the band structure in order to avoid numerical instability. The relationship between the transmission spectra and the generation order of the DPSLs is also determined. Using a gap map, a comparison is made between the traditional Bragg condition and the quasi-Bragg condition.

II. MODEL AND FORMALISM

Initially, a one-dimensional double-period dielectric superlattice, which comprises layers A and B, is considered. Both sides of the superlattice are enclosed by the same

*hsuehwj@ntu.edu.tw

semi-infinite bonding materials. All of the layers are taken to be both uniform and optically isotropic without absorption. Therefore, electromagnetic waves in the DPSL that have different polarizations are not coupled, so they can be analyzed separately. Binary layers A and B constitute DPSLs that follow the iteration rule: $A \rightarrow AB$ and $B \rightarrow AA$ [26]. According to this iteration rule, the structure S_v of a double-period superlattice of generation order $v \geq 2$ with $S_1 = A$ is $S_2 = AB$, $S_3 = ABAA$, etc. The number of layers N_v of generation order v can be calculated using $N_v = 2N_{v-1}$, for $v = 2$, where $N_1 = 1$. The refractive indices of the binary layers A and B are defined as n_A and n_B, respectively. Herein, $n_A < n_B$. The refractive index of the semi-infinite bonding media of the structure is defined as n_b. The thicknesses of layers A and B are defined as dA and dB, respectively, and these are controlled using the filling factor F of the structure as $F = dA/D$ with $D = dA + dB$. The normalized frequency is defined as Ω, where $\Omega = \omega D/2\pi c$. The incident angle of light and the period number of the structure are denoted as θ and N, respectively.

In this study, a graph model [32] is used to calculate the transmission spectra and the gap map. First, the electric and magnetic fields in the dielectric media are governed by Maxwell's curl equations. For TE polarization, the electric field in layer j, which propagates in the positive z direction, can be formulated as $\hat{E}(j,x,y,z) = \hat{y}E_y(j,x)\exp(i\omega t - i\beta z)$, where $\hat{E}$ is the electric field, $E_y(j,x)$ is the tangential electric field, and β is the propagation constant for the electric field [32]. The tangential field in layer j, $\varphi_j(x)$, which includes the electric field and the magnetic field, is governed by

$$\frac{d^2\varphi_j(x)}{dx^2} + k_j^2\varphi_j(x) = 0, \tag{1}$$

where $k_j = \pm(k_0^2 n_j^2 - \beta^2)^{1/2}$ and k_0 is the wave vector in a vacuum. By substituting the tangential electric field $E_y(j,x)$ into Eq. (1), the electric field can be expressed as the summation of the forward and backward traveling waves as

$$E_y(j,x) = a_j \exp[-ik_j(x - x_{j-1})] + b_j \exp[ik_j(x - x_{j-1})], \tag{2}$$

where A_j and B_j are the amplitudes of the forward and backward traveling waves for the tangential fields $E_y(j,x)$. According to Eq. (1), the magnetic field in layer j can be formulated as $\hat{H}(j,x,y,z) = [\hat{z}H_z(j,x) + \hat{x}H_x(j,x)]\exp(i\omega t - i\beta z)$, where $\hat{H}$ is the magnetic field. From Eq. (1), the tangential magnetic field H_z can be formulated as

$$H_z(j,x) = \frac{-k_j}{\omega\mu_0}\{-a_j \exp[-ik_j(x - x_{j-1})] + b_j \exp[ik_j(x - x_{j-1})]\}, \tag{3}$$

where μ_0 is the permeability in a vacuum. Therefore, the relationship between the electric and the magnetic fields at the interfaces of layers $x = x_{j-1}$ and $x = x_j$ can be expressed in the form: $A_j = s_j A_{j-1} + w_j B_j$ and $B_{j-1} = u_j A_{j-1} + s_j B_j$, respectively. Here, $s_j = \sec\ k_j d_j, u_j = k_j \tan\ k_j d_j, w_j = (\tan\ k_j d_j)/k_j, A_j = E_y(x_j), B_j = -i\omega\mu_0 H_z(x_j)$, and d_j is the thickness of layer j.

For a TM-polarized wave, the magnetic field in layer j that propagates in the positive z direction can be formulated in the form $\hat{H}(j,x,y,z) = \hat{y}H_y(j,x)\exp(i\omega t - i\beta z)$, where $H_y(j,x)$ is the magnetic tangential field. Using the same procedure as that for a TE-polarized wave, the relationship between the electric and the magnetic waves for different interfaces can be obtained in the same form as those for a TE-polarized wave with A_j and B_j being replaced by B_j and A_j. Here, A_j and B_j are redefined as $A_j = -i\omega\varepsilon_0 E_z(x_j)$ and $B_j = H_y(x_j)$, respectively, and ε_0 is the permittivity in a vacuum. s_j, u_j, and w_j are redefined as $s_j = \sec\ k_j d_j, u_j = (k_j/n_j^2)\tan\ k_j d_j$, and $w_j = (n_j^2 \tan\ k_j d_j)/k_j$. Using the graph method, the field between different interfaces is determined. Therefore, the transmittance, which can be verified by experiment [33], can be calculated.

In order to avoid numerical instability, the band structure is derived using the band-edge equation. According to Bloch's theorem, the electromagnetic wave in a system with a periodic boundary has the form $A_N = A_0\exp(iKL)$ and $B_N = B_0\exp(iKL)$ for an electric and a magnetic wave, respectively. L is the width of the system, and K is the Bloch wave number. From Bloch's theorem, we can obtain

$$\cos(KL) = \frac{1 - uw + s^2}{2s}. \tag{4}$$

When the Bloch wave number K is complex, $|\cos(KL)| > 1$, and light transmission is forbidden. However, when the Bloch wave number K is real, $|\cos(KL)| \leqslant 1$, and light transmission is allowed.

III. QUASI-BRAGG CONDITION

Since the QBCs for different regions are different, it is essential to determine their analytical condition. Midlines of the major gaps that are expressed as QBCs can be expressed using the following formulas. First, the ends of each major gap are classified as moving ends or fixed ends. The moving end changes, and the fixed end stays fixed if the generation order changes. Both ends of the major gaps lie on the QBC. For a gap map diagram, the region encircled by the half-wave lines $B_{A,p}$, $B_{A,p+1}$, $B_{B,q}$, and $B_{B,q+1}$ is defined as region (p,q) [19]. Here, $B_{A,p}$ and $B_{B,q}$ are half-wave lines as $k_A d_A = p\pi$ and $k_B d_B = q\pi$, where $p = 1,2,\ldots$ and $q = 1,2,\ldots$, respectively. k_A and k_B are the wave vectors of the electromagnetic wave in layers A and B, respectively. There are three major gaps in the DPSLs. Depending on the frequency range, they are defined as up, middle, and down major gaps. The QBCs of the up, middle, and the down major gaps for DPSLs in region (p,q) can be deduced from the ends of the major gaps.

For region (p,q), the left ends of the QBCs of the up, middle, and down major gaps are found at the crossing points of $k_B d_B = (q+1)\pi$ and $k_A d_A = p + [N_B^v + (-1)^{v-1}]/N_A^v\pi$, $(p + \beta_{v-1,v})\pi$, and $p\pi$, respectively. The right ends are found at the crossing points of $k_B d_B = q\pi$ and $k_A d_A = (p+1)\pi$, $[p + (N^{v-1})/N_A^v]\pi$, and $(p + \beta_{v,v})\pi$, respectively. Here, $p = 1,2,\ldots$, $q = 1,2,\ldots$, and $\beta_{v-1,v} = N_B^{v-1}/N_A^v$. N_A^v and N_B^v are the number of layers A and B of DPSLs for generation order v, which are given by $N_A^v = [2^v + (-1)^{v-1}]/3$ and $N_B^v = [2^{v-1} + (-1)^v]/3$, respectively. Therefore, the values of Ω and F for the left and right ends of a QBC of the up major gap with generation order v are

expressed as

$$(\Omega, F) = \left(\frac{\left\{p + \left[N_B^v + (-1)^{v-1}\right]/N_A^v\right\}\sigma + q + 1}{2n_B \cos\ \theta_B}, \frac{\left\{p + \left[N_B^v + (-1)^{v-1}\right]/N_A^v\right\}\sigma}{q + 1 + \left\{p + \left[N_B^v + (-1)^{v-1}\right]/N_A^v\right\}\sigma} \right) \quad \text{for left ends,} \tag{5a}$$

$$(\Omega, F) = \left[\frac{(p+1)\sigma + q}{2n_B \cos\ \theta_B}, \frac{(p+1)\sigma}{q + (p+1)\sigma} \right] \quad \text{for right ends.} \tag{5b}$$

The parameter v is not contained in Eq. (5b). Therefore, the left end of the QBC of the up major gap is a fixed end. When the generation order v changes, both the frequency and the filling factor of that end remain fixed. In contrast, the right end of the QBC of the up major gap is a moving end. The parameter v, which is contained in Eq. (5a), causes the right end of the QBC of the up major gap to change its position as the generation order v changes. Although, the QBC of the up major gaps is connected by a fixed end and a moving end, other QBCs may be different.

Using the same procedure as that for the QBC of the up major gap, both ends of the QBC of the middle major gap can be obtained from the crossing points. The left end and the right end of the QBC of the middle major gap are expressed as

$$(\Omega, F) = \left(\frac{\left[p + (N^{v-1})/N_A^v\right]\sigma + q}{2n_B \cos\ \theta_B}, \frac{\left[p + (N^{v-1})/N_A^v\right]\sigma}{q + \left[p + (N^{v-1})/N_A^v\right]\sigma} \right) \quad \text{for left ends,} \tag{6a}$$

$$(\Omega, F) = \left[\frac{(p + \beta_{v-1,v})\sigma + q + 1}{2n_B \cos\ \theta_B}, \frac{(p + \beta_{v-1,v})\sigma}{q + 1 + (p + \beta_{v-1,v})\sigma} \right] \quad \text{for right ends.} \tag{6b}$$

From Eqs. (6a) and (6b) it is seen that both ends of the QBC of the middle major gap are moving ends. The parameter v in the equation implies that the frequency and the filling factor of these ends change as the generation order v changes. From Eq. (6) it can also be deduced that neither end of the QBC of the middle major gap in one region connects with the other region. The QBC in the middle major gap of the DPSLs is discontinuous. This is different from the Bragg condition in BPSLs [25], which is continuous in different regions. Using the same procedure, the values of Ω and F for the left and right ends of the QBC of the down major gaps can be expressed in the following form:

$$(\Omega, F) = \left(\frac{p\sigma + q + 1}{2n_B \cos\ \theta_B}, \frac{p\sigma}{q + 1 + p\sigma} \right) \quad \text{for left ends,} \tag{7a}$$

$$(\Omega, F) = \left[\frac{(p + \beta_{v,v})\sigma + q}{2n_B \cos\ \theta_B}, \frac{(p + \beta_{v,v})\sigma}{q + (p + \beta_{v,v})\sigma} \right] \quad \text{for right ends.} \tag{7b}$$

The QBC of the down major gap has one moving end and one fixed end. This is similar to the situation for a QBC of the up major gap. However, the moving end of the QBC of the down major gap is the right end, and that for the QBC of the up major gaps is the left end. From Eqs. (5b) and (7a) it can also be deduced that the QBC of the up major gaps is connected with a QBC of the down major gap in another region by their fixed ends. This is different from the QBC of the middle major gap and the traditional Bragg condition.

From the trend of the above equation it can be deduced that when $v = \infty$, both ends of the up, middle, and down major gaps become fixed. For the QBC of the up major gaps, the values of Ω and F for the left and right ends of the QBCs converge to

$$(\Omega, F) = \left[\frac{(p + 1/2)\sigma + q + 1}{2n_B \cos\ \theta_B}, \frac{(p + 1/2)\sigma}{q + 1 + (p + 1/2)\sigma} \right] \quad \text{for left ends,} \tag{8a}$$

$$(\Omega, F) = \left[\frac{(p+1)\sigma + q}{2n_B \cos\ \theta_B}, \frac{(p+1)\sigma}{q + (p+1)\sigma} \right] \quad \text{for right ends.} \tag{8b}$$

As shown in Eq. (8), the parameter for the generation order v disappears from the equation. Therefore, any change in generation order no longer has an influence on either end. Only the incidence angle affects the frequency and filling factor of the ends. Note that the position of the right end of the QBC of the up major gap in Eq. (8b) is the same as that in Eq. (5b). The fixed end always remains in the same position.

The values of Ω and F for the left and right ends of the QBC of the middle major gap also converge to a certain value when the generation order is $v = \infty$. The value is expressed as

$$(\Omega, F) = \left[\frac{(p + 3/4)\sigma + q}{2n_B \cos\ \theta_B}, \frac{(p + 3/4)\sigma}{q + (p + 3/4)\sigma} \right] \quad \text{for left ends,} \tag{9a}$$

$$(\Omega, F) = \left[\frac{(p + 1/4)\sigma + q + 1}{2n_B \cos\ \theta_B}, \frac{(p + 1/4)\sigma}{q + 1 + (p + 1/4)\sigma} \right] \quad \text{for right ends.} \tag{9b}$$

The positions of the left and right ends of the QBC of the middle major gap become fixed. However, these are different from the ends in BPSLs [23]. Moreover, even if the generation order v is infinitely large and the ends of the QBC of the middle major gap are fixed, the ends in one region never connect with the ends in other regions. The QBC of the middle major gap is discontinuous, regardless of the generation order. From Eq. (7) it can be deduced that the ends of the QBC of

the down major gap also converge to a fixed value. The value of the frequency and the filling factor of them for generation order $v = \infty$ converge to

$$(\Omega, F) = \left(\frac{p\sigma + q + 1}{2n_B \cos\ \theta_B}, \frac{p\sigma}{q + 1 + p\sigma}\right) \quad \text{for left ends,} \tag{10a}$$

$$(\Omega, F) = \left[\frac{(p + 1/2)\sigma + q}{2n_B \cos\ \theta_B}, \frac{(p + 1/2)\sigma}{q + (p + 1/2)\sigma}\right] \quad \text{for right ends.} \tag{10b}$$

Again, the parameter for the generation order v vanishes from the equation when the generation order increases to infinity. The left end of the QBC of the down major gap in Eq. (10a) is the same as that in Eq. (7a). Therefore, the fixed end remains in the same position when the generation changes, and the moving end approaches a certain fixed value when the generation order increases.

From the equations for the left and right ends, the curves that pass both ends of the major gaps have the form $k_A d_A + X k_B d_B = Y\pi$. These curves are midlines of the major gaps, which are referred to as quasi-Bragg conditions for the major gaps. The QBCs for the up, middle, and down major gaps for the DPSLs in region (p,q) can be formulated as

$$k_A d_A + \alpha_v k_B d_B = (p + 1 + q\alpha_v)\pi \quad \text{for the QBC of the up major gaps,} \tag{11a}$$

$$k_A d_A + \beta_{v,v} k_B d_B = [p + \beta_{v-1,v} + \beta_{v,v}(q + 1)]\pi \quad \text{for the QBC of the middle major gap,} \tag{11b}$$

$$k_A d_A + \beta_{v,v} k_B d_B = [p + \beta_{v,v}(q + 1)]\pi \quad \text{for the QBC of the down major gap,} \tag{11c}$$

where $\alpha_v = 1 - [N_B^v + (-1)^{v-1}]/N_A^v$. Equation (11) shows that the QBCs in the DPSLs are all different from the traditional Bragg condition in BPSLs [25]. They are also different from the QBCs in Fibonacci and Thue-Morse superlattices [19,25]. When the generation order is $v = 2$, all of the QBCs become the special case $k_A d_A + k_B d_B = (p + q + 1)\pi$, which is the same as the Bragg condition in BPSLs [25]. These QBCs also approach a certain position when the generation order increases. From the trend of Eq. (11), the position of the QBC of the up, middle, and down major gaps for generation order $v = \infty$ can be deduced as

$$k_A d_A + 0.5 k_B d_B = (p + 1 + 0.5q)\pi \quad \text{for the QBC of the up major gaps,} \tag{12a}$$

$$k_A d_A + 0.5 k_B d_B = [p + 0.25 + 0.5(q + 1)]\pi \quad \text{for the QBC of the middle major gaps,} \tag{12b}$$

$$k_A d_A + 0.5 k_B d_B = [p + 0.5(q + 1)]\pi \quad \text{for QBC of the down major gaps.} \tag{12c}$$

From Eq. (12) it is seen that when the generation order is sufficiently large, the QBC approaches a fixed position.

From the QBC, the midgap centers are approached by the center at the midpoints of the QBC of the up, middle, and down major gaps, which are defined as CU, CM, and CD, respectively. The CU is found at the crossing point of $k_A d_A = (p + 1 - \gamma_v/N_A^v)\pi$ and $k_B d_B = (q + \gamma_v/N_B^v)\pi$, where $\gamma_v = \{N_A^{v-3} + [1 + (-1)^{v-1}]/4\}$. The CM is found at the crossing point of $k_A d_A = (p + 0.5)\pi$ and $k_B d_B = (q + 0.5)\pi$. The CD is found at the crossing point of $k_A d_A = (p + \gamma_v/N_A^v)\pi$ and $k_B d_B = (q + 1 - \gamma_v/N_B^v)\pi$. Their values of Ω and F can be predicted as

$$\Omega = \frac{\delta_v^p \sigma + \left(q + \gamma_v/N_B^v\right)}{2n_B \cos\theta_B}, \qquad F = \frac{\delta_v^p \sigma}{\left(q + \gamma_v/N_B^v\right) + \delta_v^p \sigma} \quad \text{for the CU,} \tag{13a}$$

$$\Omega = \frac{(p + 0.5)\sigma + (q + 0.5)}{2n_B \cos\ \theta_B}, \qquad F = \frac{(p + 0.5)\sigma}{(q + 0.5) + (p + 0.5)\sigma} \quad \text{for the CM,} \tag{13b}$$

$$\Omega = \frac{\left(p + \gamma_v/N_A^v\right)\sigma + \delta_v^q}{2n_B \cos\ \theta_B}, \qquad F = \frac{\left(p + \gamma_v/N_A^v\right)\sigma}{\delta_v^q + \left(p + \alpha_v/N_A^v\right)\sigma} \quad \text{for the CD,} \tag{13c}$$

where $\delta_v^p = p + 1 - \alpha_v/N_A^v$ and $\delta_v^q = q + 1 - \alpha_v/N_B^v$. $\sigma = n_B cos\ \theta_B/n_A cos\ \theta_A$ and θ_A and θ_B are the incident angles at layers A and B, respectively. From Eq. (13b) it is seen that the CM in the DPSLs is the same as the quarter-wave thickness for the Bragg condition for BPSLs [23]. This implies that there may be an extreme reflectance in DPSLs, similar to that in BPSLs.

From Eq. (13) it can be deduced that the CU, CM, and CB converge to simple expressions when $v = \infty$. For this condition, the Ω and F values of the CU, CM, and CB become

$$\Omega = \frac{(p + 7/8)\sigma + q + 1/4}{2n_B \cos\ \theta_B}, \qquad F = \frac{(p + 7/8)\sigma}{q + 1/4 + (p + 7/8)\sigma} \quad \text{for the CU,} \tag{14a}$$

$$\Omega = \frac{(p + 0.5)\sigma + q + 1}{2n_B \cos\ \theta_B}, \qquad F = \frac{(p + 0.5)\sigma}{q + 0.5 + (p + 0.5)\sigma} \quad \text{for the CM,} \tag{14b}$$

$$\Omega = \frac{(p + 1/8)\sigma + q + 3/4}{2n_B \cos\ \theta_B}, \qquad F = \frac{(p + 1/8)\sigma}{q + 3/4 + (p + 1/8)\sigma} \quad \text{for the CD,} \tag{14c}$$

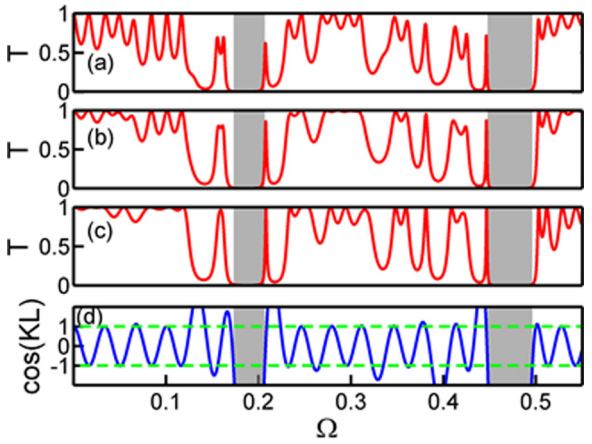

FIG. 1. (Color online) Transmission spectra for sixth-order DPSLs with (a) $n_b = n_0$, (b) $n_b = n_A$, (c) $n_b = n_B$ at normal incidence, and (d) their eigenfunction $\cos(KL)$. The normalized frequency Ω is defined by $\Omega = \omega D/2\pi c$. The parameters of the system are $n_A = 1.5$, $n_B = 2.5$, $N = 1$, $D = 1.0\ \mu$m, and $F = 0.3$. The gray areas in (a)–(d) correspond to the region of the major gaps that are sufficiently large.

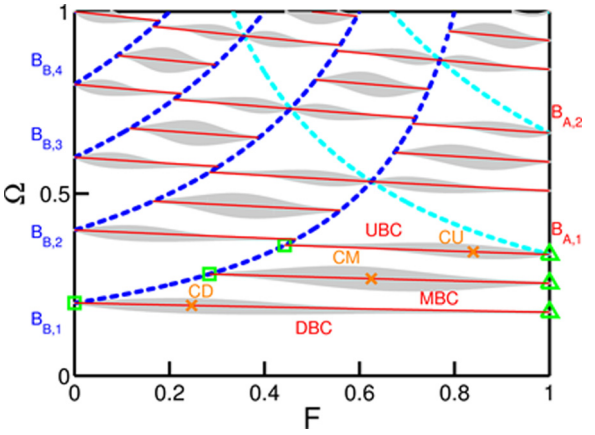

FIG. 2. (Color online) A gap map for DPSLs with $v = 6$. All of the parameters are the same as those for Fig. 1. The thickness filling factor F is defined by $F = dA/(dA + dB)$. The gray areas are major gaps. The red line marks the QBC for the major gaps. The QBCs of the up, middle, and the down major gaps for DPSLs are denoted as UBC, MBC, and DBC, respectively. The cyan (light gray) and blue (dark gray) dotted lines denote the half-wave lines $B_{A,p}$ and $B_{B,q}$, respectively. The character x represents the midpoint of the QBC in region (0,0). The squares and triangular symbols are the left and right ends in region (0,0).

respectively. The fact that the QBCs, both ends of the three major gaps, and the midpoints of the QBC approach fixed points implies that the major gaps become fixed when $v = \infty$.

IV. DISCUSSION OF RESULTS

A change in the bonding media in the DPSL changes the transmission spectra, but it has little influence on the relationship between the eigenfunction $\cos(KL)$ and the low transmission region. Figure 1 shows the relationship between the transmission spectra for different bonding media and the cosine function. The parameters of the system are $n_A = 1.5$, $n_B = 2.5$, $F = 0.3$, and $N = 1$, and the generation order is 6 at normal incidence. The gray areas in Fig. 1 denote major gaps that are sufficiently large. From Fig. 1 it is seen that the frequency range of $|\cos(KL)| > 1$ with major gaps being sufficiently large corresponds to the low transmission regions. Although the transmission changes for different bonding media, the low transmission region remains within almost the same frequency range.

Figure 2 shows the gap map for DPSLs with $v = 6$. For clarity, only the major gaps are depicted in the graph. All of the parameters in the system are the same as those for Fig. 1. The thick cyan and blue dotted lines, denoted as $B_{A,p}$ and $B_{B,q}$, are half-wave lines. The red line in Fig. 2 shows the midlines of the major gaps for the DPSLs, which account for significant reflectance due to interference. This is analogous to the Bragg condition in BPSLs. The graph shows that in each region there are three major gaps. It is seen from Fig. 2 that the QBCs for the middle major gaps in different regions are discontinuous. This result is in accordance with Eq. (12b). The cross markers are the midpoints of the QBCs. From Eq. (13b), it is seen that the CM in the DPSLs occurs for the same condition as that for BPSLs. Using the equation in Sec. II the QBCs in the gap map can be found.

When the generation order of the DPSL increases, the number of forbidden gaps increases. However, the frequency range and the gap width of the major gaps do not change significantly with the order. The existence of major gaps that are sufficiently large also has a great influence on the transmission spectra. Figure 3 shows the transmission spectrum and its corresponding major gaps for different generation orders $v = 4$–6 for the DPSLs. All of the parameters in the system are the same as those for Fig. 1 with $n_b = n_0$. The gray areas in Fig. 3 denote major gaps that are sufficiently large. The graph shows that the frequency range of the major gaps for the lower generation orders does not change significantly for higher generation orders. Furthermore, as the generation order of the DPSL increases, the transmittance in the major gaps decreases significantly. When the generation order is

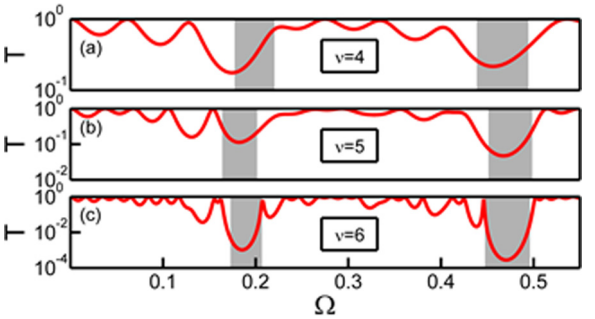

FIG. 3. (Color online) Normalized frequency and transmission spectra for DPSLs of generation orders: (a) $v = 4$, (b) $v = 5$, and (c) $v = 6$, at normal incidence. The parameters of the system are $n_A = 1.5$, $n_B = 2.5$, $n_b = n_0$, $N = 1$, $D = 1.0\ \mu$m, and $F = 0.3$. The gray areas in (a)–(c) correspond to the region of the major gaps that are sufficiently large.

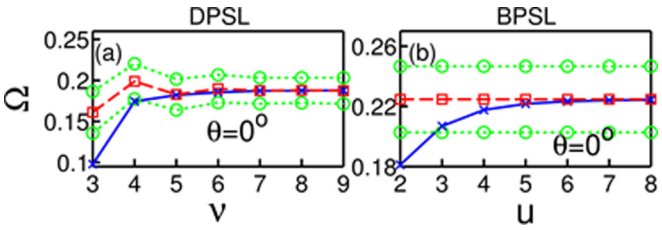

FIG. 4. (Color online) (a) The generation order v and the minimum transmittance for DPSLs at normal incidence. (b) The total number of layers 2^u and the minimum transmittance for BPSLs at normal incidence. The parameters of the system are the same as those for Fig. 3. The blue (solid) lines denote the frequency of the minimum transmittance. The green (dotted) lines and the red (dashed) lines each denote band edges and their corresponding band centers.

sufficiently large, the low transmission frequency range almost matches the frequency range of the major gaps.

Major gaps are also correlated with minimum transmittance. The minimum transmittance of the DPSLs approaches the center of the major gaps when the generation order is increased. This is similar to the case for BPSLs. Figure 4 shows the relationship between the generation order and the minimum transmittance for DPSLs and BPSLs with the same number of layers as the DPSLs at normal incidence. All of the parameters in Fig. 4 are the same as those in Fig. 3. From Fig. 4 it is seen that the frequency of the minimum transmittance of the DPSLs approaches the center of the band edges when the generation order is increased. This phenomenon is similar to that for traditional BPSLs. Therefore, the quasi-Bragg condition in

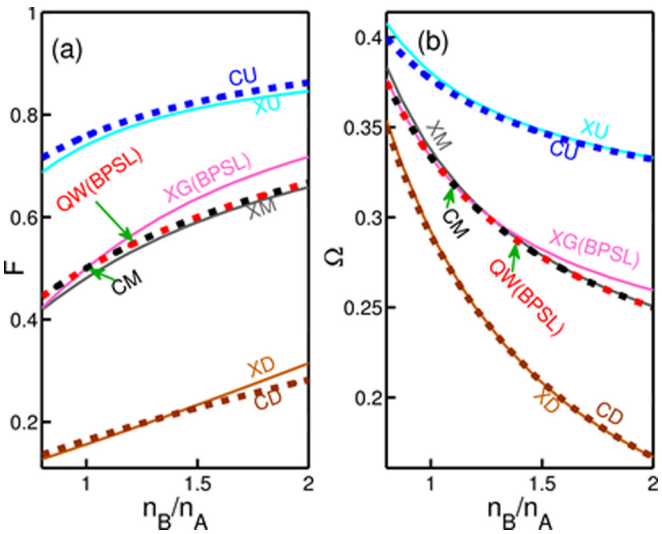

FIG. 5. (Color online) (a) The thickness filling factor and (b) the frequency of the center of the major gaps in region (0,0) for DPSLs with $v = 6$ and BPSLs with the same number of layers as the DPSLs. The parameters of the system are the same as those for Fig. 2. The dashed lines correspond to the midpoint of the QBC of the up, middle, and down major gaps of DPSLs and the quarter-wave thickness of BPSLs, denoted as CU, CM, CD, and QW(BPSL). The solid lines correspond to the maximum gap centers of the up, middle, and down major gaps of a DPSL and the major gap of a BPSL, denoted as XU, XM, XD, and XG(BPSL).

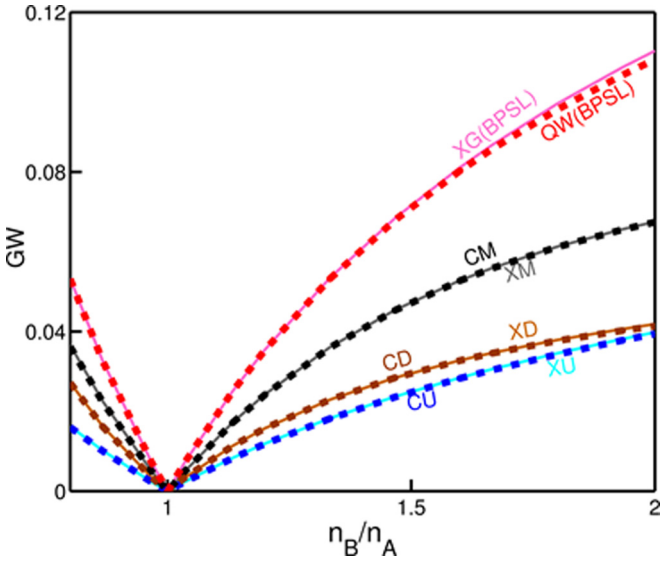

FIG. 6. (Color online) The gap width at the center of the major gaps in region (0,0) for structures that are the same as those in Fig. 5. The gap width is normalized in the same way as Ω. The parameters of the system are the same as those for Fig. 5. The dashed lines correspond to the midpoint of the QBC of the up, middle, and down major gaps of DPSLs and the quarter-wave thickness of BPSLs, denoted as CU, CM, CD, and QW(BPSL). The solid lines correspond to the maximum gap centers of the up, middle, and down major gaps of a DPSL and the major gap of a BPSL, denoted as XU, XM, XD, and XG(BPSL).

DPSLs is analogous to that for traditional BPSLs. Using the equations in Sec. III, the QBCs can be used to determine the frequency of the minimum transmittance in DPSLs.

Figure 5 shows a comparison between the position of the midpoints of the QBC and the maximum gap centers for a DPSL with $v = 6$ in region (0,0). A comparison between

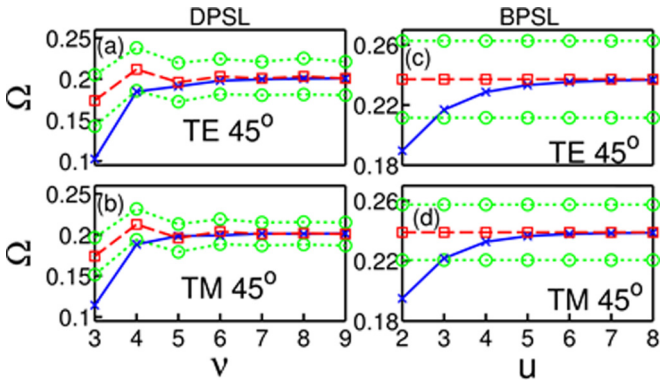

FIG. 7. (Color online) The generation order v and the minimum transmittance for DPSLs at (a) $\theta = 45°$ with TE polarization and (b) $\theta = 45°$ with TM polarization. The total number of layers 2^u and the minimum transmittance for BPSLs at (c) $\theta = 45°$ with TE polarization and (d) $\theta = 45°$ with TM polarization. The parameters of the system are the same as those for Fig. 4. The blue (solid) lines denote the frequency of the minimum transmittance. The green (dotted) lines and red (dashed) lines each denote band edges and their corresponding band centers.

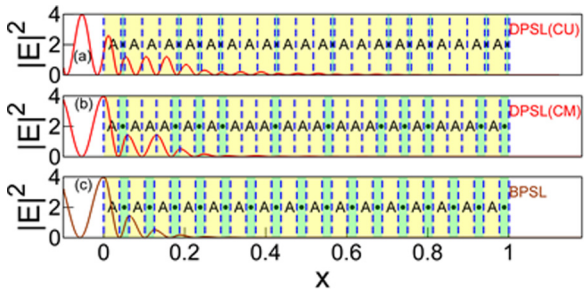

FIG. 8. (Color online) The $|E|^2$ distribution at (a) CU and (b) CM for the QBCs in DPSLs with $v = 6$. (c) The $|E|^2$ distribution at the quarter-wave thickness of BPSLs that have the same number of layers as those in Fig. 8(a). Here, $|E|^2$ is the normalized squared electric, and x is the normalized length. The parameters of the system are the same as those for Fig. 3. The (blue) dashed lines are the boundaries of the different layers. The character A (in yellow areas) and the dots (in green areas) represent materials A and B, respectively. White areas denote the bonding media where $n_b = n_0$.

the quarter-wave thickness and the maximum gap centers for BPSLs with the same number of layers as the DPSLs is also illustrated. All of the parameters in the figure are the same as those used for Fig. 2. The diagram demonstrates that in both DPSLs and BPSLs the midpoint is close to the center of the maximum gap. The midpoints and maximum gap centers for three QBCs for the DPSL are also similar to the Bragg condition for a traditional structure. Therefore, from the midpoints, the position of the maximum gap centers can be determined using Eq. (13). Figure 6 shows a comparison of the gap width between the midpoints of the QBC and the maximum gap centers for a DPSL with $v = 6$ in region (0,0). All of the parameters in the figure are the same as those used for Fig. 5. A comparison between the quarter-wave thickness and the maximum gap centers for BPSLs with the same number of layers as the DPSLs is also presented. It is shown that the gap width that is determined from the midpoints is close to the maximum gap. This result is similar to the Bragg condition for BPSLs. These QBCs are not only used to determine the high reflectance at normal incidence, but also to determine the reflectance at an arbitrary polarization angle. Figure 7 shows the relationship as those in Fig. 4 for different polarizations at 45°. All of the parameters in Fig. 7 are the same as those in Fig. 4. It can be seen in Fig. 7 that the frequency of minimum transmittance approaches the maximum gap center, regardless of the polarization or the incident angle. Since the formulas for the midpoints closely match the maximum gap center and the maximum gap closely matches minimum transmittance, a high reflection condition can be predicted using these formulas, regardless of the polarization, the incident direction, or the bonding media as shown in Fig. 1.

When traveling through the DPSLs at the QBCs, the electromagnetic wave causes significant interference and produces great reflectance. Figure 8 shows the squared electric-field profile at the CU, CM, and the quarter-wave thickness for BPSLs with the same number of layers as the DPSLs. Light propagates from the left-hand side to the right-hand side of the structure. All of the parameters in Fig. 8 are the same as those used for Fig. 3. The squared electric field approaches zero because there is destructive interference when light propagates in the structures as shown in the diagrams. From the graph it is seen that the electric field at the midpoints of the QBC for the DPSLs is analogous to the quarter-wave thickness for the Bragg condition for BPSLs.

V. CONCLUSIONS

To summarize, there are three quasi-Bragg conditions in one-dimensional double-period quasicrystals, in contrast to the single Bragg condition in traditional periodic cases. Three analytical formulas for these quasi-Bragg conditions are proposed, and the results match significant reflectance. The QBCs for DPSLs are discontinuous in each region. The frequency and the thickness filling factor at the ends of each QBC are derived. The results show that these QBCs are different not only from those in Fibonacci and Thue-Morse superlattices, but also from the Bragg condition in a traditional periodic system. These three midpoints of the QBCs that correspond to the maximum reflectance are found in double-periodic systems. At the midpoint of each QBC, the squared electric field decreases to almost zero when light propagates in the double-periodic superlattices because of interference. These three thickness conditions where the maximum reflections occur at the midpoints of the QBCs in the DPSLs are analogous to the quarter-wave condition for a periodic system. These quasi-Bragg conditions suggest the application of double-period superlattices on narrow-band multiwavelength optical filters and random lasers. These results may be extended to the study of optical, electronic, magnetic, and other fields.

ACKNOWLEDGMENTS

The authors acknowledge the support, in part, by the National Science Council of Taiwan under Grant Nos. NSC 102-2221-E-002-105 and MOST 103-3113-E-002-001.

[1] A. Yariv and P. Yeh, *Optical Waves in Crystals: Propagation and Control of Laser Radiation* (Wiley, New York, 1984).
[2] Y. V. Shvyd'ko, S. Stoupin, A. Cunsolo, A. H. Said, and X. Huang, Nat. Phys. **6**, 196 (2010).
[3] J. Ristić, E. Calleja, A. Trampert, S. Fernández-Garrido, C. Rivera, U. Jahn, and K. H. Ploog, Phys. Rev. Lett. **94**, 146102 (2005).
[4] B. S. Williams, Nat. Photonics **1**, 517 (2007).
[5] Y. Taniyasu, M. Kasu, and T. Makimoto, Nature (London) **441**, 325 (2006).
[6] D. Shechtman, I. Blech, D. Gratias, and J. W. Cahn, Phys. Rev. Lett. **53**, 1951 (1984).
[7] E. Abe, Y. Yan, and S. J. Pennycook, Nature Mater. **3**, 759 (2004).

[8] J. Mikhael, J. Roth, L. Helden, and C. Bechinger, Nature (London) **454**, 501 (2008).
[9] W. J. Hsueh, C. T. Chen, and C. H. Chen, Phys. Rev. A **78**, 013836 (2008).
[10] R. W. Peng, M. Wang, A. Hu, S. S. Jiang, G. J. Jin, and D. Feng, Phys. Rev. B **57**, 1544 (1998).
[11] M. Kohmoto, B. Sutherland, and K. Iguchi, Phys. Rev. Lett. **58**, 2436 (1987).
[12] Y. H. Cheng and W. J. Hsueh, Opt. Lett. **38**, 3631 (2013).
[13] S.-W. Wang, X. Chen, W. Lu, M. Li, and H. Wang, Appl. Phys. Lett. **90**, 211113 (2007).
[14] T. Y. L. Ang and M.-K. Chin, Opt. Express **17**, 5176 (2009).
[15] P. A. Kalozoumis, C. Morfonios, N. Palaiodimopoulos, F. K. Diakonos, and P. Schmelcher, Phys. Rev. A **88**, 033857 (2013).
[16] Z. V. Vardeny, A. Nahata, and A. Agrawal, Nat. Photonics **7**, 177 (2013).
[17] H. S. Sözüer and K. Sevim, Phys. Rev. B **72**, 195101 (2005).
[18] R. W. Peng, Y. M. Liu, X. Q. Huang, F. Qiu, M. Wang, A. Hu, S. S. Jiang, D. Feng, L. Z. Ouyang, and J. Zou, Phys. Rev. B **69**, 165109 (2004).
[19] W. J. Hsueh, C. H. Chang, Y. H. Cheng, and S. J. Wun, Opt. Express **20**, 26618 (2012).
[20] F. A. B. F. de Moura and M. L. Lyra, Phys. Rev. Lett. **81**, 3735 (1998).
[21] H. Shima, T. Nomura, and T. Nakayama, Phys. Rev. B **70**, 075116 (2004).
[22] M. Dulea, M. Severin, and R. Riklund, Phys. Rev. B **42**, 3680 (1990).
[23] Y. Fink, J. N. Winn, S. Fan, C. Chen, J. Michel, J. D. Joannopoulos, and E. L. Thomas, Science **282**, 1679 (1998).
[24] E. Yablonovitch, Opt. Lett. **23**, 1648 (1998).
[25] C. W. Tsao, W. J. Hsueh, C. H. Chang, and Y. H. Cheng, Opt. Lett. **38**, 4562 (2013).
[26] M. S. Vasconcelos and E. L. Albuquerque, Phys. Rev. B **59**, 11128 (1999).
[27] S. R. Entezar and H. Rahimi, Opt. Commun. **284**, 5833 (2011).
[28] M. Enrique, Rep. Prog. Phys. **75**, 036502 (2012).
[29] M. S. Vasconcelos, P. W. Mauriz, F. F. de Medeiros, and E. L. Albuquerque, Phys. Rev. B **76**, 165117 (2007).
[30] L. Mahler, A. Tredicucci, F. Beltram, C. Walther, J. Faist, H. E. Beere, D. A. Ritchie, and D. S. Wiersma, Nat. Photonics **4**, 165 (2010).
[31] R. W. Peng, X. Q. Huang, F. Qiu, M. Wang, A. Hu, S. S. Jiang, and M. Mazzer, Appl. Phys. Lett. **80**, 3063 (2002).
[32] W. J. Hsueh, S. J. Wun, Z. J. Lin, and Y. H. Cheng, J. Opt. Soc. Am. B **28**, 2584 (2011).
[33] F. Qiu, R. W. Peng, X. Q. Huang, Y. M. Liu, M. Wang, A. Hu, and S. S. Jiang, Europhys. Lett. **63**, 853 (2003).